Solid Freeform Fabrication 2021: Proceedings of the 32nd Annual International Solid Freeform Fabrication Symposium – An Additive Manufacturing Conference
Reviewed Paper

Effects of Heat Treatment and Fast Neutron Irradiation on the Microstructure and Microhardness of Inconel 625 Fabricated via Laser-Powder Bed Fusion

T. Keya[1], V. O'Donnell[2], J. Lieben[1], A. Romans[1], G. Harvill[1],
M. Andurkar[3], J. Gahl[2], S.M. Thompson[3], and B. C. Prorok[1]

[1]Department of Materials Engineering, Auburn University, Auburn, AL 36849
[2]University of Missouri Research Reactor (MURR), University of Missouri, Columbia, MO 65211
[3]Alan Levin Department of Mechanical & Nuclear Engineering, Kansas State University, Manhattan, KS 66506

Abstract

The microstructure of Inconel 625 fabricated via Laser-Powder Bed Fusion (L-PBF) was investigated in as-printed and heat-treated conditions. The very high cooling rates inherent to the L-PBF process generally result in fine microstructures and complex residual stress fields which requires annealing to reduce stress and tailor the microstructure to obtain the desired mechanical properties. Inconel 625 alloy, a nickel-based superalloy, continues to be a common material employed with the L-PBF process. The unique microstructure produced by the L-PBF process and different phases introduced by different heat treatment processes require investigation to facilitate the material's wide range of applications. This paper investigates the influence of heat treatments at 700°C, 900°C and 1050°C for one hour on the microstructure and microhardness of the L-PBF parts. The parts were irradiated using 'fast' neutrons in University of Missouri Research Reactor Center (MURR). The microhardness before and after radiation are also compared.

1. Introduction

Laser Powder Bed Fusion (L-PBF) offers the ability to fabricate metal parts with highly-customized geometries, tailored structures and consolidated assemblies. This additive manufacturing (AM) method has several advantages of traditional manufacturing methods, including, fabrication-friendly environments promoting lean production by reducing material waste, fabrication of parts made from a broad range of materials including superalloys, and reduction of fabrication time and cost [1-2]. During the L-PBF process, a focused high-energy laser beam selectively melts a powder layer accompanied with rapid cooling/solidification for a predetermined shape defined via computer aided drawing (CAD) data. This process is followed by the coating of a new powder layer that is melted selectively to the previous layer. This cycle goes on until the final product is completely manufactured. During L-PBF, very high heat fluxes are imposed for creation of a melt pool which results in very high thermal gradients within the heat affected zone [3]. These thermal gradients manifest into significant residual stress distributions. During solidification, cooling rates can be as high as 10^3 K/s to 10^6 K/s, whereas for traditional methods, e.g. casting, has a cooling rate on the order of 1 to 10^3 K/s [4]. These complex thermo-mechanical phenomena lead to fine dendritic inhomogeneous microstructures that require

investigation; often to determine how an L-PBF material performs relative to its wrought counterparts.

Inconel 625 (Alloy 625, IN625) is a nickel superalloy with exceptionally superior mechanical properties that derives its strength from solid solution strengthening by chromium (Cr), molybdenum (Mo) and niobium (Nb) atoms [4, 5]. In addition to solid solution strengthening, IN625 exhibits precipitation hardening primarily from the precipitation of the fine metastable γ″ phase. It is suitable for high temperature applications and is corrosion resistant making it an ideal candidate for aerospace, medical or energy sectors.

Researchers have reported formation of γ″, δ, Pt_2Mo-type phase, Laves phase and carbides in the typical FCC γ matrix of IN625 [6]. Floreen et al. reported formation of γ″ precipitates at 593°C-760°C and formation of Laves and δ precipitates at 704°C-982°C in wrought IN625 [6]. The stable δ phase, which can be needle or plate shaped, is formed upon dissolution of metastable γ″ precipitate due to local rises in Nb content [7,8]. Dinda et al. studied the microstructure of IN625 fabricated via Laser aided Directed Energy Deposition (L-DED) and reported a stable dendritic structure, even at 1000°C [9]. Hu et al. found reduced ductility with increasing temperature in L-PBF IN625 [10]. This decrease in ductility is caused by intergranular cracking due to inhomogeneous microstructure introduced by the L-PBF process. Stoudt et al. reported faster precipitation in L-PBF IN625 compared to wrought material [11]. The nature of the L-PBF process causes localized concentration of Nb and Mo atoms that acts as the driving force to form δ precipitates at 870°C in as quickly as 15 minutes. δ phase formation can be controlled by a stress relieving heat treatment and modifying Nb and Mo content. Another study on forged, L-PBF and Laser Melting Deposition (LMD) IN625 revealed heterogeneous microstructure with columnar dendrites in the latter two [12]. The microstructure in L-PBF IN625 is finer and more textured than that found in the forged and LMD microstructures. The L-PBF microstructure can contribute to a material's superior hardness and strength, as well as its poor ductility relative to wrought material. Heat treatment of IN625 parts at 1100°C makes the mechanical properties more comparable to that of wrought parts. The superior mechanical properties found in L-PBF IN625 may also be attributed to high dislocation density along with the fine dendritic microstructure [13]. Marchese et al. reported formation of γ″ precipitates and Cr-rich carbides after heat treating L-PBF IN625 at 700°C for 24 hours which caused high strength with poor ductility. Recrystallization occurred after annealing the material at 1150°C for 2h resulting in dissolution of precipitates and a mixture of large as well as fine grains. Li et al. also reported high dislocation density as well as high residual stress in L-PBF IN625 [14]. In addition, the precipitation of the δ phase at 800°C and 900°C was found to result in higher hardness [14]. Precipitates or carbides usually are not found in as-built L-PBF IN625 [15]. Decrease in lattice constant after heat treatment was also found which is attributed to significant carbide precipitation.

A detailed investigation of effects of nuclear radiation on microstructure and mechanical properties of AM IN625 can facilitate use of this alloy in nuclear reactors. Related studies found embrittlement and increase in hardness due to irradiation induced defects and precipitation. Hashimoto et al. conducted a study on ion irradiated Inconel 718 that was traditionally manufactured, solution annealed (SA) and precipitation hardened (PH) [16]. Samples were irradiated using Fe^+, He^+ and H^+ beams of different strength at 200°C. Nanoindentation on irradiated samples revealed an increase in hardness for both SA and PH conditions. Higher dose and He injection on SA samples induced larger concentration of Frank loops and cavities resulting in irradiation-induced hardening. In Fe irradiated PH IN718, softening occurred due to incoherent γ′ and γ″ precipitates. In He irradiated PH samples, hardening was observed with increasing He

concentration for up to 14 at%, then softening occurred at 20 at% He concentration due to dissolution of precipitates. Another study on Nimonic PE-16 (another nickel-based superalloy) alloy also emphasizes on He embrittlement over γ′ precipitation hardening [17]. Angeliu et al. suggested reduction in helium concentration and solute segregation to control radiation hardening [18]. Song et al. presented a comprehensive study on proton irradiated stainless steel, Ni based alloys and ferritic alloys [19]. Most samples showed formation of voids, dislocation loops and precipitates upon irradiation at 360°C and 2.5 dpa. IN625 experienced enrichment of Cr and Mo on grain boundaries and precipitation of Pt_2Mo-type phase induced by the irradiation. Ni-based alloys found to be more prone to radiation damage compared to ferritic alloys. Cieslik et al. reported traditionally manufactured IN625 to be more resistant to ion irradiation compared to its L-PBF counterpart [20]. Softening occurred for wrought alloy with increase in fluence whereas L-PBF IN625 experienced softening at 1.0 dpa and hardening at 3.0 dpa. The nano-hardness of the as-built L-PBF IN625 was found to be about 8% higher than that of wrought IN625 before irradiation. Increase in hardness for wrought IN625 was about 3%, but there was 6% increase in hardness for L-PBF IN625 after irradiation at 0.1 dpa. Softening at 1.0 dpa can possibly be attributed to grain growth and migration of defects such as voids, loops, and dislocations. Fincher et al. suggested post-radiation annealing to alleviate some radiation damage in solution annealed IN718 [21]. In-situ annealing at 300°C-500°C for short period of time can relieve embrittlement induced by H^+ and Ni^{2+} ions to some extent.

The objective of this research work is to investigate the effects of different heat treatment schedules comprising of 700ºC, 900ºC, 1050ºC for 1 hour on the microstructure and micro-hardness of IN625 fabricated by L-PBF. Metallurgical characterization is carried out on as-printed and heat-treated samples to analyze formation of precipitates. Fast neutron irradiation was conducted on another similarly processed set of samples and micro-hardness was measured afterwards. Finally, sample hardness data were compared before and after irradiation. There is lack of studies that focus on microstructure and mechanical properties of additively manufactured IN625 irradiated by fast neutrons. This study will provide a better understanding of microstructural evolution of L-PBF IN625 before and after heat treatment and open doors to further investigate the effects of fast neutron irradiation on as-printed and heat-treated L-PBF IN625 for facilitating their use in low nuclear attenuation applications.

2. Experimental Methods

2.1 Material and L-PBF Process Parameters

A Concept Laser MLab Cusing 100R L-PBF AM systems was used to produce all IN625 specimens. The AM machine was equipped with a 100 W fiber laser that has a wavelength of 1070 nm. The build volume of the machine measures 90 x 90 x 80 mm. Cubes with dimensions of 10x10x10 mm^3 were additively manufactured. The laser power was set to 90 W with a scan speed of 800 mm/s. The laser diameter was 80 µm and the layer thickness is set to 25 µm with a hatch spacing of 60 µm. A density of 99.79% was achieved with these parameters. The compositions of the Inconel 625 powder used for L-PBF and the wrought Inconel 625 are indicated in Table 1.

Table 1: Elemental composition of Inconel 625 powder (% in weight)

Element	Ni	Cr	Mo	Fe	Nb+Ta	Co	C	P	S	Al	Ti	Mn
% wt	Bal	21	9	<5.0	3.5	<1.0	< 0.1	<0.015	<0.015	<0.4	<0.4	<0.5

2.2 Heat Treatment

After separating the specimens from the built plate, each of them was exposed to a different heat treatment except one that was kept in the as-printed condition. Heat treatments were performed at 700°C, 900°C and 1050°C for 1h each. Temperature inside the furnace was measured using a K-type thermocouple and all samples were air cooled.

Heat treatment parameters were chosen for precipitation of the metastable γ″ and stable δ phase. Fig. 1(a) shows the complete TTT diagram for wrought IN625 [22] and Fig. 1(b) shows the thermal exposure conditions for δ formation in additively manufactured IN625 compared to wrought IN625 [11]. It may be seen from Fig. 1(b) that the time for δ phase formation for the same temperature is drastically reduced for the AM-LPBF samples compared to wrought. This behavior can be explained by the segregation of solute elements during solidification, which increases the probability for secondary phase formation. During L-PBF, the cooling rates are much higher than those experienced during conventional processes. This is known to lead to a finer dendritic structure with smaller dendrite spacing. Zhang et al. showed that L-PBF produces a finer microstructure for IN625 than other AM processes (Electron Beam Melting and L-DED) and that the cellular/columnar substructures are enriched in Mo and Nb, while Ni and Cr are deficient [23].

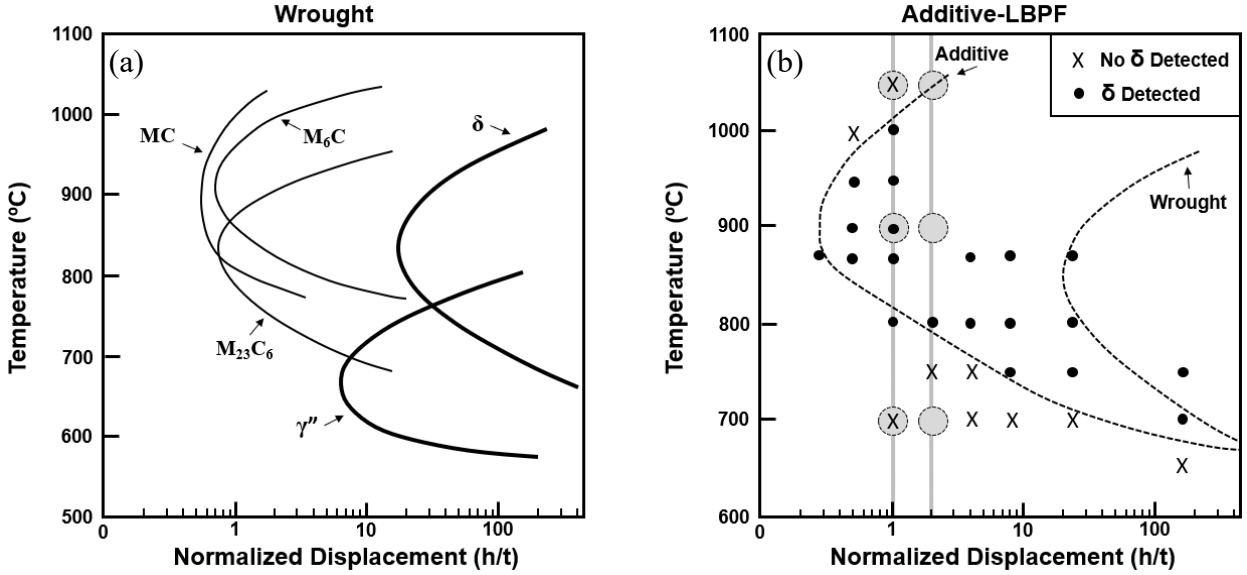

Figure 1: (a) Time-Temperature-Transformation (TTT) diagram of IN625, adapted from [22], (b) TTT diagram comparing the presence of δ-phase in additively manufactured IN625 to the wrought material. The dashed lines estimate approximately 1 %-volume fraction of δ-phase, adapted from [11]

2.3 Metallographic Sample Preparation

Specimens were sectioned parallel to the build direction and hot mounted on CONDUCTOMOUNT™ mounting resin. Grinding and polishing were carried out on each sample

down to 0.25 μm colloidal silica suspension. To reveal microstructure, samples were electro-etched with 70% phosphoric acid at 3-5 volts for 5-40 seconds.

2.4 Characterization Techniques

Scanning Electron Microscopy (SEM) was used to characterize microstructure before and after heat treatment on L-PBF specimens. A JEOL 7000F SEM unit was used to take high magnification images of the microstructure of the samples. Vickers hardness was also measured using a Phase-II Micro Vickers Hardness Tester before and after heat treatment and fast neutron irradiation.

2.5 Irradiation

A 25-week irradiation study was conducted on polished L-PBF samples in the as-printed and heat-treated conditions. 'Fast' neutrons produced from a cyclotron (GE PETtrace) at University of Missouri Research Reactor Center (MURR). This experiment looked at hardness value changes in the samples as the irradiations progressed. Samples were periodically removed for hardness testing over the course of the experiment to track variations. Samples were placed in a cyclotron vault, next to a fluorine-18 production target. The neutron flux inside the cyclotron vault had been modeled, showing that the neutrons resulting from the $^{18}O(p, n)^{18}F$ reaction have energies of 0.4 MeV to 16.5 MeV, and that the neutron flux in the vault is, conservatively, between 1.8×10^9 and 3.0×10^9 n cm^{-2} s^{-1} [24]. To standardize the results, the neutron flux was converted to 1 MeV equivalent neutrons, resulting in an equivalent flux between 2.4×10^9 and 4.0×10^9 n cm^{-2} s^{-1} of mono-energetic neutrons.

3. Results and Discussion

3.1 Microstructure: As-printed condition

Microstructures of the as-printed L-PBF IN625 specimens are shown in Fig. 2. Typical 'U' or 'C' shaped melt pools related to the laser scanning process are visible on the surface parallel to build direction. Although it is difficult to measure the exact width due to overlapping, the width of the melt pool is about 100-120 μm. The overlapping is also a result of the employed hatch spacing, thus resulting in relatively high density with no gaps between melt pools. This morphology is formed when the material rapidly solidify after melting by the laser source as soon as the laser moves. Li et al. also reported similar morphology that is more 'V' shaped resembling welding tracks [15]. The angle of the 'V' is a function of laser scanning speed and any increase in scanning speed decreases the angle and the melt pool becomes narrower.

At higher magnification, cellular and columnar grains can be observed as shown in Fig. 2(b). This may indicate growth of dendrites in different directions. An overall columnar growth along build direction is found as indicated by arrows on Fig. 2(b). The growth of the dendritic structure through melt pools is shown in Fig. 2(c). The dendrites are about 500 nm wide with Nb and Mo segregation on an interdentritic region and a Ni- and Cr-rich dendritic core as reported by other studies [14, 23].

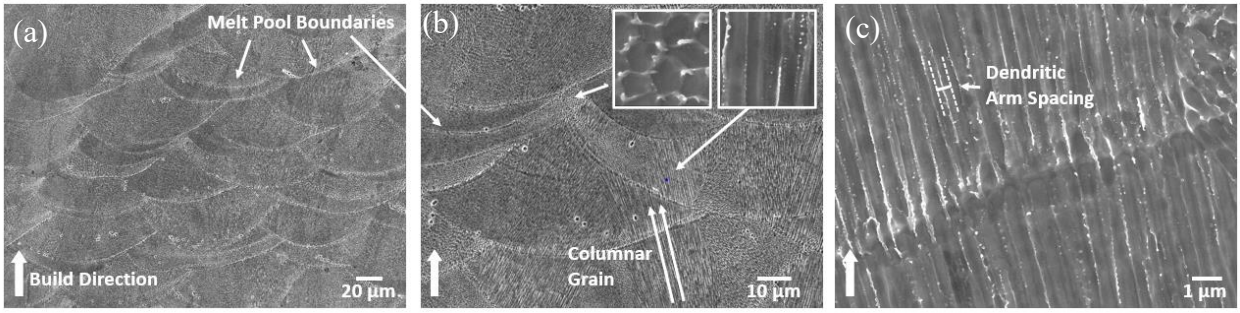

Figure 2: SEM micrographs of as-printed L-PBF IN625 after electro-etching, (a) Melt pools on the plane parallel to build direction, (b) Cellular and dendritic microstructure at higher magnification, (c) Dendritic growth through melt pool boundaries at higher magnification.

3.2 Microstructure: Heat Treated at 700°C

Microstructure of the L-PBF specimens after 1 hour heat treatment at 700ºC are shown in Fig. 3. At lower magnification, melt pools are noticeable after 1h (Fig. 3a) and it looks very similar to the as-printed microstructure (Fig. 2a). Dendritic microstructure and elemental segregation at the interdendritic region are more evident at higher magnification (Fig. 3b-c). These observations agree with other studies performed L-PBF IN625 [11, 13, 15]. Several research groups reported formation of metastable γ″ precipitate in the range of 550-750°C [6-7, 25-28]. γ″ precipitate has a tetragonal structure with composition of Ni_3(Nb, Ti, Al). These precipitates can be plate, disc, lens, spherical or elliptical shaped. It can take a long time to form γ″ phase in traditionally manufactured IN625, but precipitation may occur as soon as in 1h in AM materials [15]. Some areas observed in fig. 3(a, b) appear to be deficient of precipitation which may be attributed to elemental inhomogeneity throughout the sample. Areas with Nb depletion may not be able to form γ″ precipitates as carbides like NbC forms [6]. Precipitation is also affected by Ti content in the material.

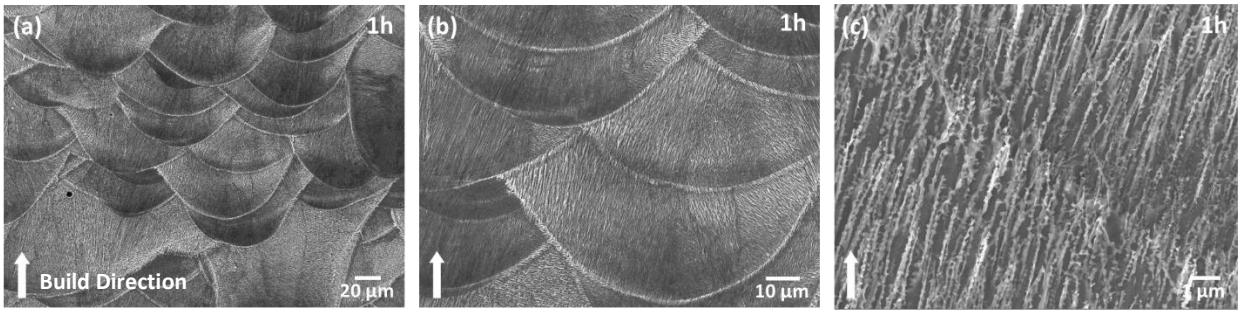

Figure 3: SEM micrographs of L-PBF IN625 after heat treating at 700°C for 1 hour; (a) Melt pools on the surface parallel to build direction, (b) Melt pools with cellular and columnar growth at higher magnification, (c) Precipitation at interdendritic region.

3.3 Microstructure: Heat Treated at 900°C

Fig. 4 presents the microstructure after heat treatment at 900ºC for 1h. Remnants of the melt pools can still be observed after 1h of heat treatment (Fig. 4a, b). While some precipitation is evident in certain areas, some areas have been recrystallized due to the dissolution of elemental segregation/precipitation that exist in the as-printed and 700°C heat treated conditions. Plate and needle shaped particles are formed along sub-grain boundaries after 1h that resemble δ phase as shown in Fig. 4c [6, 29]. δ precipitates have orthorhombic structure with composition of Ni_3Nb or

Ni_3(Nb, Mo) [6, 25]. It can be acicular, plate or globular shaped, although acicular, thin rod or needle shaped particles are most common. It is easier to detect and separate δ particles from its unique morphology. Laves phase forms at around the same temperature range in IN625, but it has a "blocky" irregular shape and its formation in IN625 is limited due to lower Fe content compared to IN718 [6]. Stable δ phase forms from metastable γ″ precipitates when it dissolves into the matrix leaving high local concentration of Nb atoms [15, 29]. It usually starts forming at grain boundaries, then spreads out throughout the grain. Researchers have reported formation of δ phase formation at 650-982℃ [6, 25, 28, 29]. As can be seen from the TTT diagrams in Fig. 1, longer time might be required if the temperature is relatively low to form the precipitates. Baldan et al. reported evident formation of δ phase at 725℃ after 500h for traditionally manufactured IN625 [29]. Also shown in fig. 1, δ precipitates form much faster in AM materials compared to wrought IN625. Due to the nature of the L-PBF process, there is Nb enrichment along interdendritic regions that triggers formation of precipitates that are Cr deficient, but enriched with larger Nb and Mo atoms [4]. Stoudt et al. reported formation of δ particles in L-PBF IN625 at 870℃ after 15 minutes [11]. Lass et al. reported formation of plate shaped δ precipitates at 870℃ for 1h in L-PBF IN625 [4].

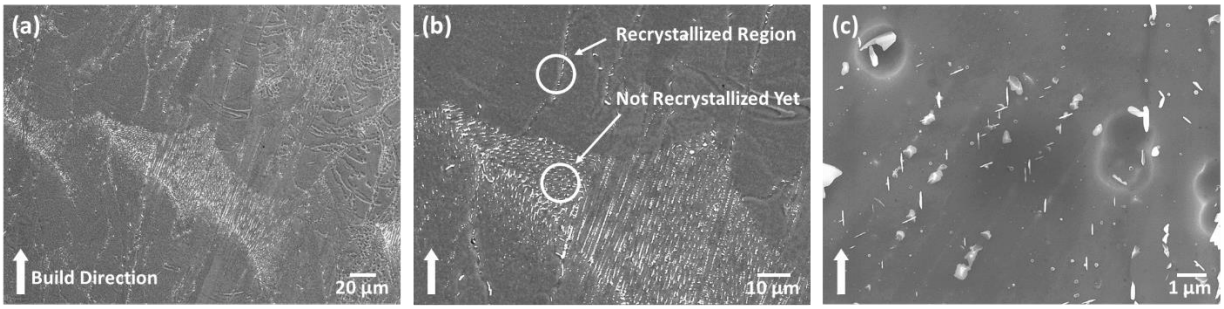

Figure 4: SEM micrographs of L-PBF IN625 after heat treating at 900℃ for 1 hour; (a) Melt pools on the plane parallel to build direction, (b) Columnar microstructure at higher magnification, (c) Precipitation in columnar regions.

3.4 Microstructure: Heat Treated at 1050℃

Microstructure of heat-treated sample at 1050℃ for 1h is presented in Fig. 5. Melt pool boundaries, dendrites, elemental segregation, and most precipitates disappear at this heat treatment temperature causing complete recrystallization. Equiaxed grains with some annealing twins are visible. Presence of annealing twins indicates release of some residual stress that formed due to rapid cooling during the L-PBF process [12, 14]. Although not investigated in this study, some irregular block shaped MC, M_6C or other carbides might be present after this heat treatment temperature [13, 15, 25, 26]. These carbides are often randomly distributed and have no specific orientation relative to the γ matrix [7]. Melt pools, precipitates and dendrites disappear usually at temperatures above 1000℃ [6, 12, 15]. Sufficient recrystallization with some primary carbides is reported to occur at 1150℃ in L-PBF IN625 [13,14, 15, 23].

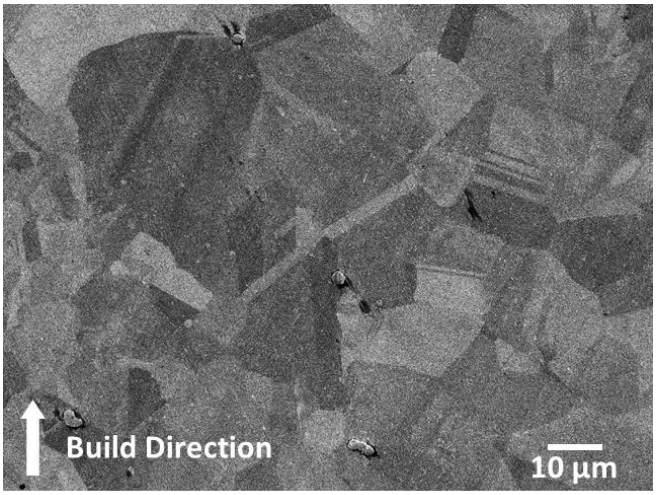

Figure 5: SEM micrographs of L-PBF IN625 after heat treatment at 1050℃ for 1h.

3.5 Hardness: Before and After Irradiation

Vickers hardness data for the as-printed and heat treated samples before and after irradiation are shown in Fig. 6. It may be seen that the pre-irradiation hardness of the as-printed L-PBF sample is about 340.50±6.06 HV which is close to literature values [12, 15]. It is much higher than wrought IN625 which is about 260±5 HV [12]. The high cooling rates during the L-PBF process cause "trapping" of Nb and Mo atoms and this phenomenon builds up residual stress in the material resulting in higher hardness compared to wrought or forged IN625 [12, 14, 15].

Heat treating at 700℃ for 1h increases pre-irradiation hardness by about 5% which indirectly indicates γ″ precipitation [12]. Hardness before irradiation keeps decreasing with increases in temperature. Although δ precipitate causes hardening of material [15], the hardness decreases at 900℃. The effect of γ″ dissolution, release of residual stress and increase of grain size may dominate over that of δ phase formation [12, 14]. The hardness decreases at 1050℃ and becomes 266.6±5.02 HV which is close to wrought IN625 values found in the literature [12]. This phenomenon is caused by dissolution of precipitates and increase in grain size [12, 14, 15].

As-printed and heat-treated L-PBF samples were irradiated using fast neutrons produced at MURR. Over the course of the experiment, hardness values of the samples were measured intermittently, as summarized in Fig. 6. The post-irradiation hardness of all samples display both softening and hardening, but they are relatively consistent after a fluence of 2.05×10^{15} n/cm^2. All samples saw notable changes between the initial pre-irradiation measurements and the measurement taken after 8.57×10^{14} n/cm^2 fluence. After that, hardness values did not show much change. Relevant studies are not available that investigate effect of fast neutron irradiation on the microstructure and mechanical properties of L-PBF IN625, but some have reported irradiation hardening due to formation and rearrangement of defects and precipitates in the material [19, 20, 30, 31]. The presence of both hardening and softening effects is not uncommon [31]. Irradiation can give rise to local strain causing formation of loops that promote hardening [30]. It can also promote formation and growth of precipitates [19]. Defects like voids, loops or interstitials can form and accumulate resulting in increased hardness. On the other hand, dissolution of precipitates, increase in grain size, or resettling of the defects can cause softening [20].

The 1-MeV-equivalent neutron fluence at the end of the 25 weeks was 9×10^{15} n/cm^2. This fluence would be considered low for a typical material damage study but was enough to get

preliminary results that show this method of fast neutron irradiation is viable for future experiments.

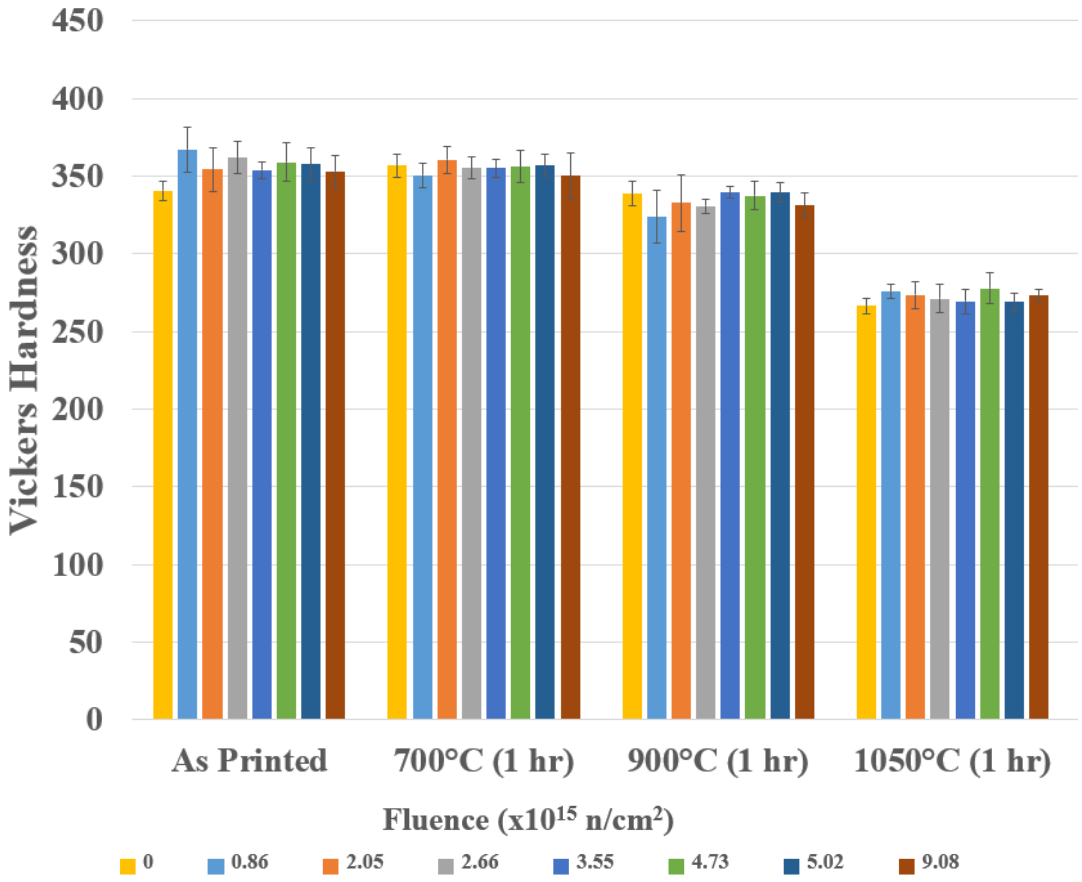

Figure 6: Vickers hardness as function of accumulated neutron fluence for L-PBF specimens.

4. Conclusions

The microstructure and microhardness of L-PBF IN625 before and after heat treatment have been investigated in this study. The microhardness after fast neutron irradiation is also presented and compared. Some important observations from this study are outlined below:

1. L-PBF produces fine dendritic microstructure in IN625 that grows along the build direction due to rapid cooling.
2. Melt pool boundaries and interdendritic segregation are retained through heat treatment at 700°C. At 900°C, melt pools start to dissolve and intergranular precipitation can be observed.
3. Melt pools, elemental segregation and precipitates are dissolved at 1050°C and equiaxed grains with annealing twins are formed.
4. As-printed L-PBF IN625 has higher hardness compared to wrought IN625.
5. L-PBF samples heat treated at 700°C for 1h displayed the highest hardness among all samples before irradiation, whereas 1050°C sample showed the lowest hardness among L-PBF samples and most comparable to wrought IN625.

6. Both hardening and softening occur in L-PBF IN625 during continuous exposure to fast neutrons up to 9×10^{15} n/cm² normalized fluence.

L-PBF technology can be a very powerful tool for modern nuclear reactor applications, but extensive research is required to investigate the performance of materials like IN625 with a complex microstructure produced using the technology. This study sheds light on evolution of microstructure of L-PBF produced IN625 superalloy in as-printed and heat-treated conditions at various temperatures which can be very useful to explain its mechanical properties like microhardness. Hardness after irradiation is also investigated after different levels of fluence which is a step forward towards understanding the performance of L-PBF IN625 in low nuclear attenuation applications.

Acknowledgement

This material is based upon work supported by the U.S. Department of Energy's Office of Nuclear Energy under Award Number DE-NE0008865.

Disclaimer

References

1. Huang, S.H., Liu, P., Mokasdar, A. and Hou, L., 2013. Additive manufacturing and its societal impact: a literature review. *The International Journal of Advanced Manufacturing Technology*, *67*(5), pp.1191-1203.
2. Klahn, C., Leutenecker, B. and Meboldt, M., 2015. Design strategies for the process of additive manufacturing. *Procedia Cirp*, *36*, pp.230-235.
3. Kruth, J.P., Froyen, L., Van Vaerenbergh, J., Mercelis, P., Rombouts, M. and Lauwers, B., 2004. Selective laser melting of iron-based powder. *Journal of Materials Processing Technology*, *149*(1-3), pp.616-622.
4. Lass, E.A., Stoudt, M.R., Williams, M.E., Katz, M.B., Levine, L.E., Phan, T.Q., Gnaeupel-Herold, T.H. and Ng, D.S., 2017. Formation of the Ni 3 Nb δ-phase in stress-relieved IN625 produced via laser powder-bed fusion additive manufacturing. *Metallurgical and Materials Transactions A*, *48*(11), pp.5547-5558.
5. Reed, R.C., 2008. *The superalloys: fundamentals and applications*. Cambridge university press.

6. Floreen, S., Fuchs, G.E. and Yang, W.J., 1994. The metallurgy of alloy 625. *Superalloys*, *718*(625), pp.13-37.
7. Sundararaman, M., Mukhopadhyay, P. and Banerjee, S., 1988. Precipitation of the δ-Ni 3 Nb phase in two nickel base superalloys. *Metallurgical Transactions A*, *19*(3), pp.453-465.
8. Jambor, M., Bokůvka, O., Nový, F., Trško, L. and Belan, J., 2017. Phase transformations in nickel base superalloy INCONEL 718 during cyclic loading at high temperature. *Production Engineering Archives*, *15*(15), pp.15-18.
9. Dinda, G.P., Dasgupta, A.K. and Mazumder, J., 2009. Laser aided direct metal deposition of Inconel 625 superalloy: Microstructural evolution and thermal stability. *Materials Science and Engineering: A*, *509*(1-2), pp.98-104.
10. Hu, X.A., Zhao, G.L., Liu, F.C. and Liu, W.X., 2019. Microstructure and mechanical behavior of IN625 alloy processed by selective laser melting at high temperature up to 1000° C. *Rare Metals*, pp.1-9.
11. Stoudt, M.R., Lass, E.A., Ng, D.S., Williams, M.E., Zhang, F., Campbell, C.E., Lindwall, G. and Levine, L.E., 2018. The influence of annealing temperature and time on the formation of δ-phase in additively-manufactured IN625. *Metallurgical and Materials Transactions A*, *49(7),* pp.3028-3037.
12. Nguejio, J., Szmytka, F., Hallais, S., Tanguy, A., Nardone, S. and Martinez, M.G., 2019. Comparison of microstructure features and mechanical properties for additive manufactured and wrought nickel alloys 625. *Materials Science and Engineering: A, 764*, p.138214.
13. Marchese, G., Lorusso, M., Parizia, S., Bassini, E., Lee, J.W., Calignano, F., Manfredi, D., Terner, M., Hong, H.U., Ugues, D. and Lombardi, M., 2018. Influence of heat treatments on microstructure evolution and mechanical properties of IN625 processed by laser powder bed fusion. *Materials Science and Engineering: A, 729*, pp.64-75.
14. Li, C., White, R., Fang, X.Y., Weaver, M. and Guo, Y.B., 2017. Microstructure evolution characteristics of IN625 alloy from selective laser melting to heat treatment. *Materials Science and Engineering: A, 705,* pp.20-31.
15. Li, S., Wei, Q., Shi, Y., Zhu, Z. and Zhang, D., 2015. Microstructure characteristics of IN625 superalloy manufactured by selective laser melting. *Journal of Materials Science & Technology, 31(9),* pp.946-952.
16. Hashimoto, N., Hunn, J.D., Byun, T.S. and Mansur, L.K., 2003. Microstructural analysis of ion-irradiation-induced hardening in inconel 718. *Journal of Nuclear Materials, 318*, pp.300-306.
17. Boothby, R.M., 1996. The microstructure of fast neutron irradiated Nimonic PE16. *Journal of Nuclear Materials, 230(2),* pp.148-157.
18. Angeliu, T.M., Ward, J.T. and Witter, J.K., 2007. Assessing the effects of radiation damage on Ni-base alloys for the prometheus space reactor system. *Journal of Nuclear Materials, 366(1-2),* pp.223-237.
19. Song, M., Lear, C.R., Parish, C.M., Wang, M. and Was, G.S., 2018. Radiation tolerance of commercial and advanced alloys for core internals: a comprehensive microstructural characterization. *Journal of Nuclear Materials, 510*, pp.396-413.
20. Cieślik, I., Duchna, M., Płociński, T., Wyszkowska, E., Azarov, A. and Zieniuk, M., 2020. Ion irradiation effect on the microstructure of Inconel 625 obtained by Selective Laser Melting and by the metallurgical process. *Surface and Coatings Technology, 396*, p.125952.

21. Fincher, C.D., Turman, H., French, A., Chancey, M., Gigax, J., Aydogan, E., Zhao, D., Yadav, D., Xie, K., Wang, Y. and Borden, M., 2020. Damage relief of ion-irradiated Inconel alloy 718 via annealing. *Nuclear Instruments and Methods in Physics Research Section B: Beam Interactions with Materials and Atoms, 479*, pp.157-162.
22. Shoemaker, L.E., 2005. Alloys 625 and 725: trends in properties and applications. *Superalloys, 718(625),* pp.409-418.
23. Zhang, F., Levine, L.E., Allen, A.J., Campbell, C.E., Lass, E.A., Cheruvathur, S., Stoudt, M.R., Williams, M.E. and Idell, Y., 2017. Homogenization kinetics of a nickel-based superalloy produced by powder bed fusion laser sintering. *Scripta Materialia, 131*, pp.98-102.
24. Jeffries, B., Algiere, C., Gallagher, J., Nichols, T., So, J., Littlefield, C., Quinn, M. and Brockman, J., 2019. Characterization of the neutron flux during production of 18F at a medical cyclotron and evaluation of the incidental neutron spectrum for neutron damage studies. *Applied Radiation and Isotopes, 154*, p.108892.
25. Shankar, V., Rao, K.B.S. and Mannan, S.L., 2001. Microstructure and mechanical properties of Inconel 625 superalloy. *Journal of Nuclear Materials, 288(2-3),* pp.222-232.
26. Rai, S.K., Kumar, A., Shankar, V., Jayakumar, T., Rao, K.B.S. and Raj, B., 2004. Characterization of microstructures in Inconel 625 using X-ray diffraction peak broadening and lattice parameter measurements. *Scripta Materialia, 51(1),* pp.59-63.
27. Mukherjee, P., Sarkar, A., Barat, P., Jayakumar, T., Mahadevan, S. and Rai, S.K., 2006. Lattice misfit measurement in Inconel 625 by X-ray diffraction technique. *arXiv preprint cond-mat/0604222*.
28. Suave, L.M., Cormier, J., Villechaise, P., Soula, A., Hervier, Z., Bertheau, D. and Laigo, J., 2014. Microstructural evolutions during thermal aging of alloy 625: impact of temperature and forming process. *Metallurgical and Materials Transactions A, 45(7),* pp.2963-2982.
29. Baldan, R., Silva, A.A.A.P.D., Tanno, T.M., Costa, E.T.D., Brentegani, J.V.N. and Couto, A.A., 2020. Experimental Investigation of Delta Phase Precipitation in Inconel 625 Superalloy Aged at 550, 625 and 725° C. *Materials Research, 23(1).*
30. Was, G.S., 2016. Fundamentals of radiation materials science: metals and alloys. springer.
31. Byun, T.S., Garrison, B.E., McAlister, M.R., Chen, X., Gussev, M.N., Lach, T.G., Le Coq, A., Linton, K., Joslin, C.B., Carver, J.K. and List, F.A., 2021. Mechanical behavior of additively manufactured and wrought 316L stainless steels before and after neutron irradiation. *Journal of Nuclear Materials, 548*, p.152849.
32. O'Brien, M.J., 2019. Development and qualification of additively manufactured parts for space. *Optical Engineering*, *58*(1), p.010801.